Selective Mechanical Transfer of Graphene from Seed Copper Foil Using Rate Effects

Seung Ryul Na,[†,#] Ji Won Suk,[⊥,#] Li Tao,[§] Deji Akinwande,[§] Rodney S. Ruoff,[‡,∥] Rui Huang,[†] and Kenneth M. Liechti*[,†]

[†]Department of Aerospace Engineering and Engineering Mechanics, Research Center for the Mechanics of Solids, Structures and Materials, [‡]Department of Mechanical Engineering and The Materials Science and Engineering Program, and [§]Department of Electrical and Computer Engineering, The University of Texas at Austin Austin, Texas 78712, United States, [∥]Institute of Basic Sciences Center for Multidimensional Carbon Materials & Department of Chemistry and School of Materials Science and Engineering Ulsan National Institute of Science and Technology, Ulsan 689-798, Republic of Korea, and [⊥]School of Mechanical Engineering, Sungkyunkwan University, Suwon 440-746, Republic of Korea. [#]These authors (S.R.N. and J.W.S.) contributed equally to this work.

ABSTRACT A very fast, dry transfer process based on mechanical delamination successfully effected the transfer of large-area, CVD grown graphene on copper foil to silicon. This has been achieved by bonding silicon backing layers to both sides of the graphene-coated copper foil with epoxy and applying a suitably high separation rate to the backing layers. At the highest separation rate considered (254.0 μm/s), monolayer graphene was completely transferred from the copper foil to the target silicon substrate. On the other hand, the lowest rate (25.4 μm/s) caused the epoxy to be completely separated from the graphene. Fracture mechanics analyses were used to determine the adhesion energy between graphene and its seed copper foil (6.0 J/m^2) and between graphene and the epoxy (3.4 J/m^2) at the respective loading rates. Control experiments for the epoxy/silicon interface established a rate dependent adhesion, which supports the hypothesis that the adhesion of the graphene/epoxy interface was higher than that of the graphene/copper interface at the higher separation rate, thereby providing a controllable mechanism for selective transfer of graphene in future nanofabrication systems such as roll-to-roll transfer.

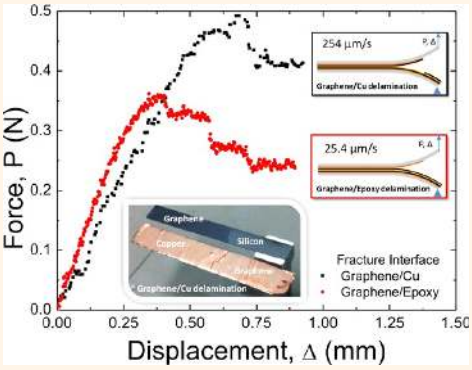

KEYWORDS: graphene · copper · epoxy · mechanical transfer · selective transfer · adhesion energy · traction-separation relations · rate effects

Dry transfer of graphene has been an integral part of its history from the earliest days when scotch tape was first used to exfoliate graphene from graphite.[1] This approach produces relatively small flakes with single or multiple layers. Chemical vapor deposition of graphene on thin (~35 μm) large area copper foils,[2−4] and related metal foils such as commercially available Cu−Ni foils,[5] produces large area graphene, up to meters in the in-plane dimension.[6] Graphene has also been grown on copper film (~1 μm thick)[7] that has been deposited on silicon wafers.

No matter which approach to the deposition of large area graphene is taken, the same problem remains: transferring the graphene to its destination substrate for the myriad of applications that are currently being considered. Some applications may require intermediate carrier films to be used, so several contact and separation events can be expected. In most cases, the adhesive interactions that are involved in contact and separation are assumed to be van der Waals in nature, but the details could vary significantly depending on the contact pair and environmental effects.[8] The strongest interactions may be between graphene and its seed metal; interactions between graphene and target substrates are expected to be weaker but may be modified by surface functionalization. The effort that is featured here relates to the most challenging interface at this stage in our development; removing graphene from its seed copper foil, which is an attractive substrate for roll-to-roll nanomanufacturing processes. Doubts about being able to meet this dry transfer challenge have led

* Address correspondence to kml@mail.utexas.edu.

Received for review September 12, 2014 and accepted February 3, 2015.

Published online February 03, 2015
10.1021/nn505178g

to so-called "wet transfer" where the seed copper foil is etched away[9] or an electrochemical process[10] that generates bubbles at the graphene/copper foil interface and separates the graphene from the foil. Yoon *et al.*[11] were the first to demonstrate that graphene could be mechanically separated from its seed copper layer. In that work, the copper film had been deposited on silicon oxide prior to CVD of graphene. A second silicon strip was bonded to the graphene with an epoxy. The two silicon strips were peeled apart and, for applied displacement rates above 5.0 μm/s, it was shown that delamination occurred along the graphene/seed copper interface, transferring a graphene monolayer onto the epoxy.

In this work, we demonstrate, for the first time, how graphene can be mechanically separated from its seed copper foil and dry transferred to a target substrate. By sandwiching the graphene-coated copper foil between two silicon strips and separating the assembly over a wide range of peeling rates, we have been able to establish that it is possible to control when the graphene/copper or the graphene/epoxy interface delaminates. The latter is useful when contemplating subsequent transfer steps where the graphene might need to be removed from the polymer backing layer. These demonstrations are supplemented by measurements of the strength and range of the interactions associated with each interface as well as the adhesion energy.

RESULTS AND DISCUSSION

Graphene/Copper Delamination. Graphene-coated copper foils[2] were sandwiched between silicon strips with an epoxy as the adhesive. The ends of the upper and lower silicon strips were separated (Figure 1a) under displacement control with rates ranging from 25.4 to 254.0 μm/s. As the stitched image in Figure 1b indicates, it was possible to obtain clean transfer of graphene over a 16 $\times$ 5 mm^2 region starting from the epoxy terminus, when the applied displacement rate was 254.0 μm/s. A more detailed view of the contrast that graphene provides is shown in Figure 1c at the epoxy terminus. The dark region is indicative of graphene on epoxy, while the gray region is the lower surface of the upper silicon strip that did not have any epoxy and consequently no graphene on it. An even higher magnification view of the corresponding region on the surface of the copper foil (Figure 1d) reveals that graphene also provided contrast on copper. The mainly lighter region in the top portion of the figure is where the graphene was removed from the copper; some groups of lines corresponding to steps on the surface of the copper foil can be seen here. Note that some graphene (darker islands) was not removed from the copper, mainly near the epoxy terminus. On the other hand, the mainly darker region in the lower half, corresponding to the region where no epoxy had contacted the upper silicon strip or the graphene on the foil, shows that the graphene coverage was uniform in this region. The straight line features are wrinkles in the graphene and the small darker regions are ad-layers where additional graphene islands were grown on the monolayer graphene during growth.

A more detailed view of the graphene-coated surface of the epoxy is presented in Figure 2a. The steps and wrinkles that were observed on the bare copper surface were replicated by the relatively low viscosity epoxy. In addition, there were holes in the graphene which exposed bare epoxy as islands and led to local charging effects. The distribution of holes in the graphene was bimodal, with larger holes mainly within regions surrounded by wrinkles and much smaller ones along the wrinkles. The larger holes in the graphene appear to have occurred during the transfer process as also indicated by the graphene patches left behind on the copper fracture surface (Figure 1d). On other hand, the smaller holes in the graphene along the wrinkles may correspond to defects caused by wrinkling during growth. The initial state of the graphene on copper foil following deposition is captured in Figure 2b-c. The grain boundaries of the copper and steps within the copper grains are clearly visible (Figure 2b). Wrinkles in the graphene following growth are again present and are accompanied by small dark spots along the wrinkles. Experience has shown that these spots are copper oxide that is formed by oxygen passing through very small defects induced by the wrinkles and oxidizing the bare copper beneath. Nonetheless, the coverage of the copper by the graphene was quite complete. There were no grain boundaries present in Figure 2c, because the image was taken inside a large copper grain. However, some defects that were larger than the copper oxide spots appeared at some locations near the wrinkles. The conclusion from these images is that graphene was well-transferred to the epoxy, with a slightly higher defect count, particularly within regions surrounded by wrinkles. Nonetheless, as will be borne out later by Raman maps and electrical resistance measurements, these defects did not impair the overall quality of the graphene.

On the basis of the SEM micrographs just described, the fracture path at an applied displacement rate of 254.0 μm/s is shown schematically in Figure 3a. The stress concentration provided by the bimaterial corner between the epoxy terminus and the graphene (Supporting Information Figure S2) caused a crack to penetrate the graphene and then grow along the graphene/copper interface. The corresponding load–displacement response is shown in Figure 3b, where the first peak and load drop correspond to the initiation and growth of a fast crack from the bimaterial corner. The specimen was then unloaded, thereby arresting the crack and providing a sharp crack for

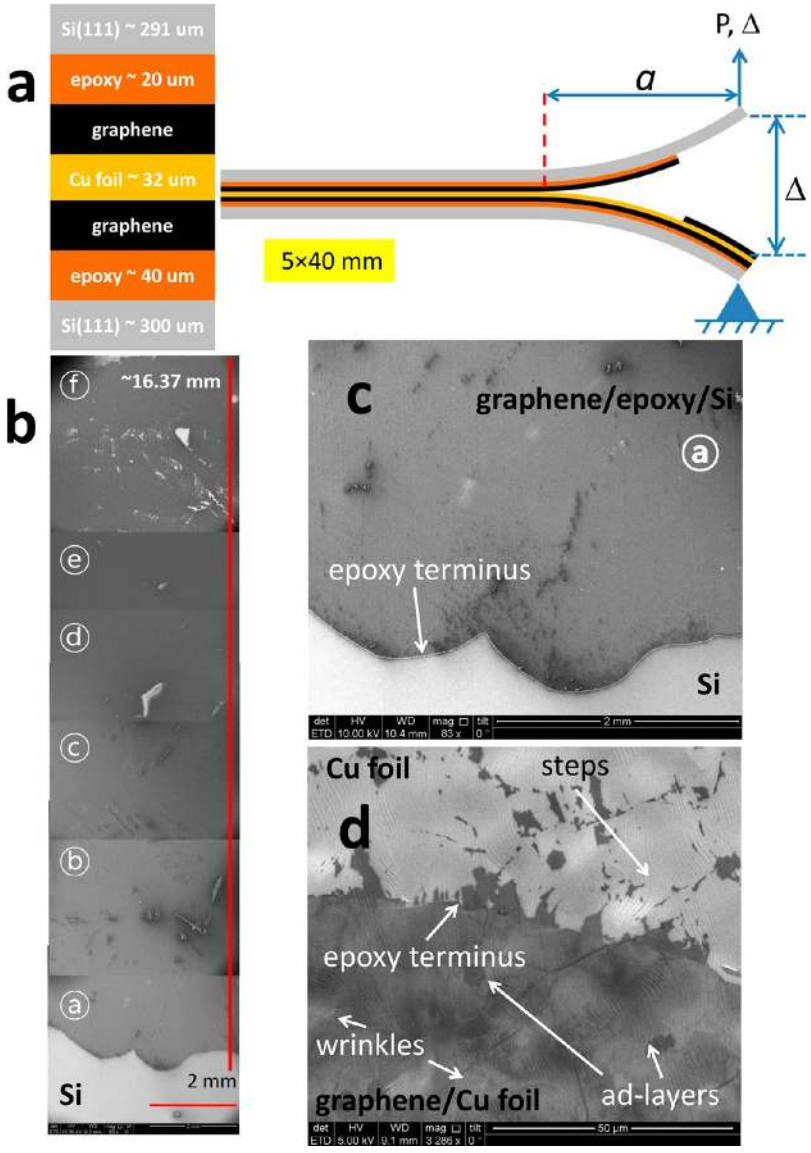

Figure 1. Schematics of the cross section of the specimen and experimental configuration are presented along with low- and high-resolution SEM images of the fracture surfaces. (a) Cross section and a specimen under load. The crack length *a* is defined as the distance from the crack front to the loading point. (b) Low-resolution, stitched SEM images of graphene transferred to the epoxy. (c) High-resolution SEM image of epoxy on silicon near the epoxy terminus after graphene transfer. (d) High-resolution SEM of copper foil near the epoxy terminus after transfer.

the subsequent reloading. This time, the onset of crack growth was followed by slower, more stable growth which transitioned to fast cracking prior to the next unloading for cycle 3, where the sequence was repeated.

While SEM micrographs of the graphene coated epoxy surface are indeed useful for determining the areal extent of graphene transfer, Raman spectroscopy (Figure 3c) is required for determining the quality of the transferred graphene. Thirteen spots on approximately 1 mm centers along the graphene-coated epoxy surface were probed. All the Raman spectra exhibited G and 2D peaks at approximately 1600 and 2700 cm^{-1}, respectively. The peak at approximately 1600 cm^{-1} was made up of two peaks as can be seen in the decomposed spectrum (Supporting Information Figure S5): the G peak for graphene at 1587 cm^{-1} and a major peak at 1605 cm^{-1} from the epoxy.[8] The graphene spectrum also exhibited the 2D peak at 2691 cm^{-1}, thereby verifying the presence of the graphene on the epoxy. While the average intensity ratio I_{2D}/I_G was 1.89, indicating that monolayer graphene had indeed been grown on the copper foil, the average value of the intensity ratio I_{2D}/I_G for graphene in the decomposed spectrum was 1.3. Note the slight shifts in the G and 2D peaks on the epoxy and copper; taking the latter as a reference, it is possible that the shift that occurred upon transferring the graphene to the epoxy was due to residual stresses and substrate effects.[12,13] There was a D band peak at 1353 cm^{-1} for

the 12th spot, which indicates that there was some damage to the graphene at this location. A set of 8 Raman spectra were obtained from the opposite fracture surface. The first five had no G or 2D peaks, thereby confirming that the graphene had indeed been removed from that portion of the copper foil. The spots marked 6, 7, and 8 had G and 2D peaks at 1580 and 2709 cm^{-1}, respectively, as they probed that part of the copper foil which had not been covered by epoxy. The point wise spectra were augmented by a series of Raman maps, which have been presented in detail in Section 12 of Supporting Information. These confirmed the conclusions obtained by SEM and point wise Raman spectra. As a final measure of the effective transfer of graphene from the seed copper to the epoxy, the sheet resistance of the graphene was measured using the transfer length method (TLM). Details are provided in Section 14 of Supporting Information. The sheet resistance was 863.6 Ω/□. The sheet resistance was at the lower end of the range for graphene that had been transferred to PMMA using a conventional wet transfer process.[14]

To our knowledge, this is the first time that large area, CVD grown graphene has been mechanically removed from its seed-copper foil and dry transferred to another substrate. Compared to wet transfer, the potential for speeding up graphene transfer in nanomanufacturing processes such as roll-to-roll transfer by such a mechanical approach is clear. An additional advantage is that the copper foil can potentially be recovered and recycled in the same roll-to-roll process.[11]

Graphene/Epoxy Delamination. At an applied displacement rate of 25.4 μm/s, the picture was quite different; the crack grew at the graphene/epoxy interface. As indicated in the schematic (Figure 4a), the crack initiated at the bimaterial corner (Supporting Information Figure S2) and propagated along the graphene/epoxy interface without ever breaking the graphene monolayer itself. The corresponding load−displacement response is shown in Figure 4b. Only one loading cycle was applied, but there were clear signs of slow crack growth prior to the peak load, at which point the crack growth became faster with some indications of stick−slip behavior. There was no 2D peak in any of the 10 Raman spectra (Figure 4c) that were taken on the epoxy side of the fracture surface. They all had peaks near 1605 cm^{-1}, but these are attributable to the epoxy itself.[8] Raman maps were also obtained of the epoxy fracture surface as described in Section 13 of the Supporting Information. They confirmed the conclusions from the point wise spectra. However, both G and 2D peaks were present at 1590 and 2710 cm^{-1}, respectively, in the 9 Raman spectra that were taken at a series of spots on the graphene-coated copper foil. The average value of the intensity ratio I_{2D}/I_G from the 9 spectra was 2.4, again indicating that monolayer

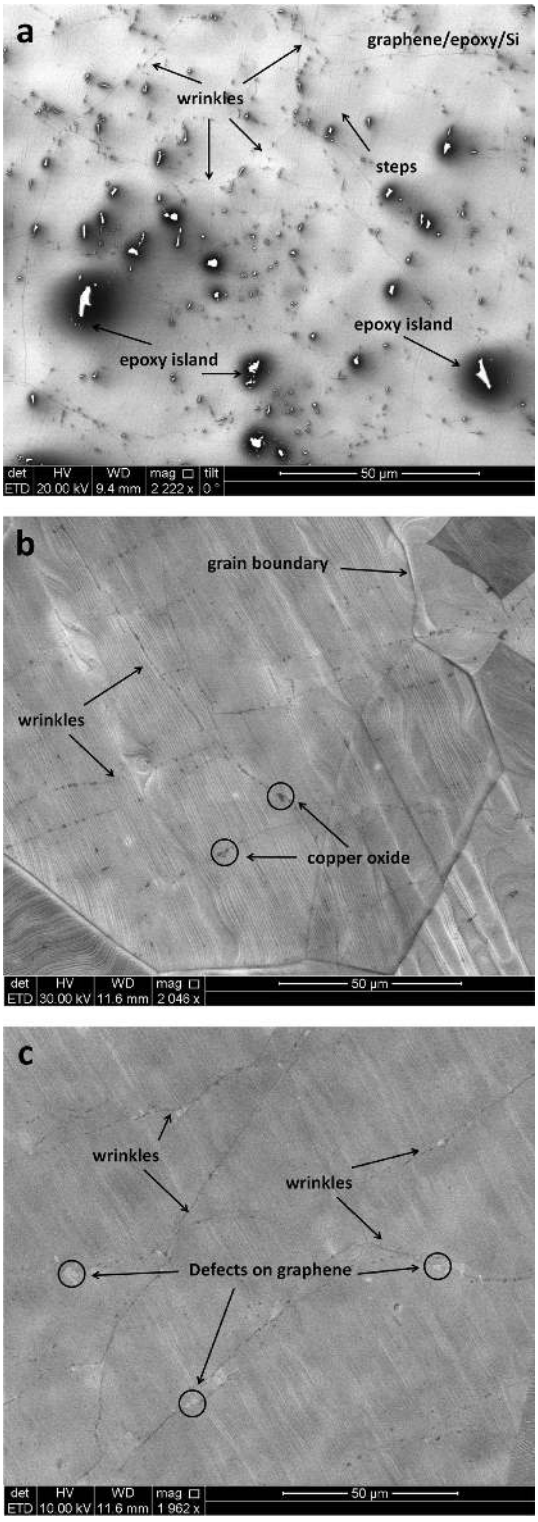

Figure 2. High-resolution SEM images of graphene transferred to epoxy and on copper following growth. (a) Following transfer, steps, ad-layers, wrinkles, and epoxy islands or holes in the graphene can be seen on the epoxy fracture surface. Before transfer, (b) graphene wrinkles, copper oxide, grain boundaries and steps can be seen on the copper. (c) Another region contains notable defects (most likely holes) in addition to graphene wrinkles and copper steps.

graphene was present before and after delamination between the graphene and epoxy. The peaks were

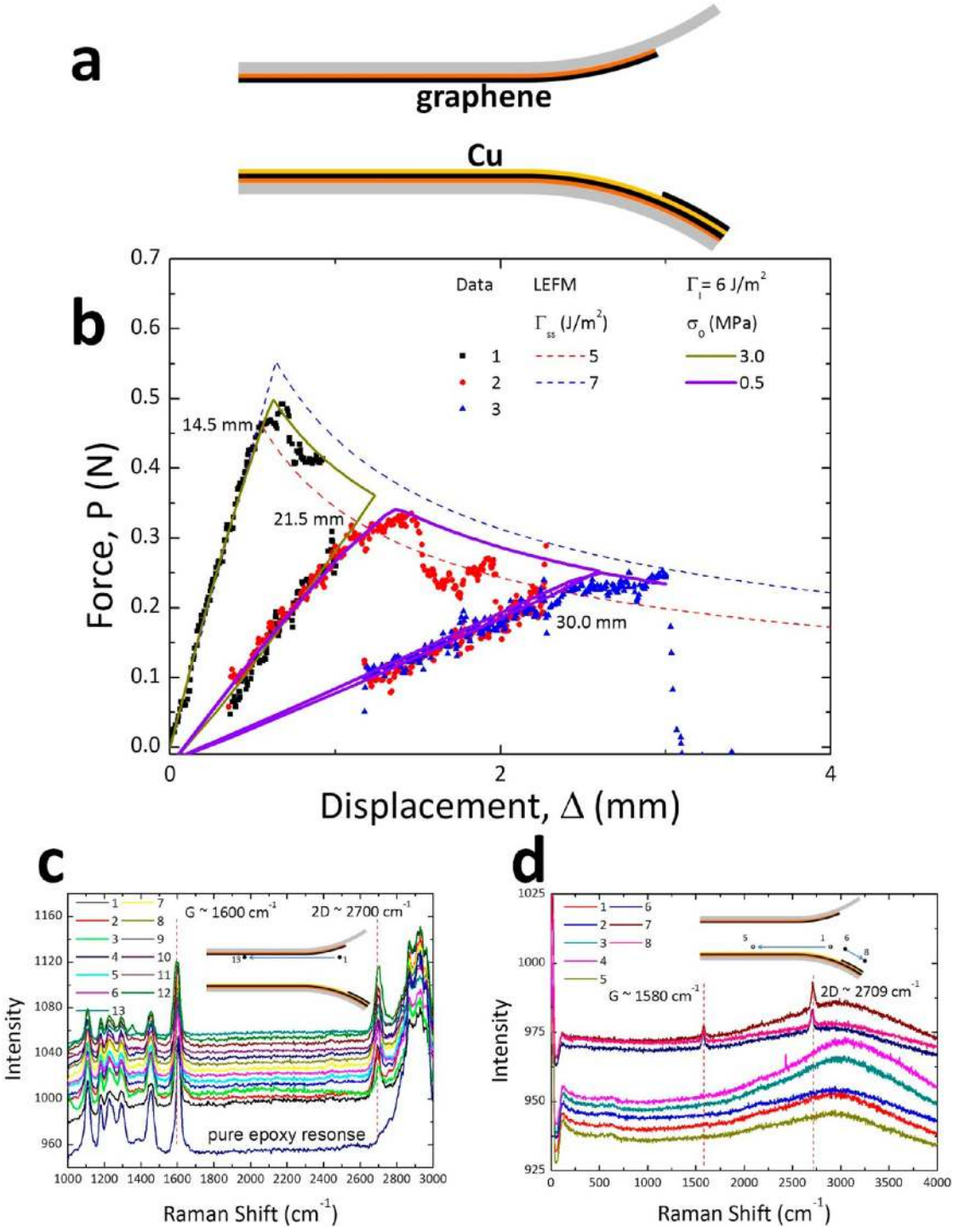

Figure 3. Results of experiments at an applied separation rate of 254.0 μm/s. (a) A schematic of delamination along the graphene/copper interface. (b) Force−displacement response of three experiments and associated simulations. (c) Raman spectra of graphene transferred on epoxy and pure epoxy. (d) Raman spectra of copper foil after mechanical transfer; the series of spots from 1 to 5 shows no graphene because it was transferred to the epoxy, while spots 6 to 8 indicate the presence of graphene in the pre crack region where there was no epoxy.

slightly shifted from those obtained from as-grown graphene on copper foil (Figure 4d), again suggesting a residual stress in the graphene after delamination. This might have been due to plastic deformation in the copper foil as the crack front passed by a particular location, leaving behind residual strain in a plastic wake partly or entirely through the thickness of the copper foil. It is also possible that the orientation of copper grains and strains on graphene shifts Raman peaks.[15−17] However, no such shifts were observed in Raman spectra that were obtained from graphene that had just been deposited on copper foil.

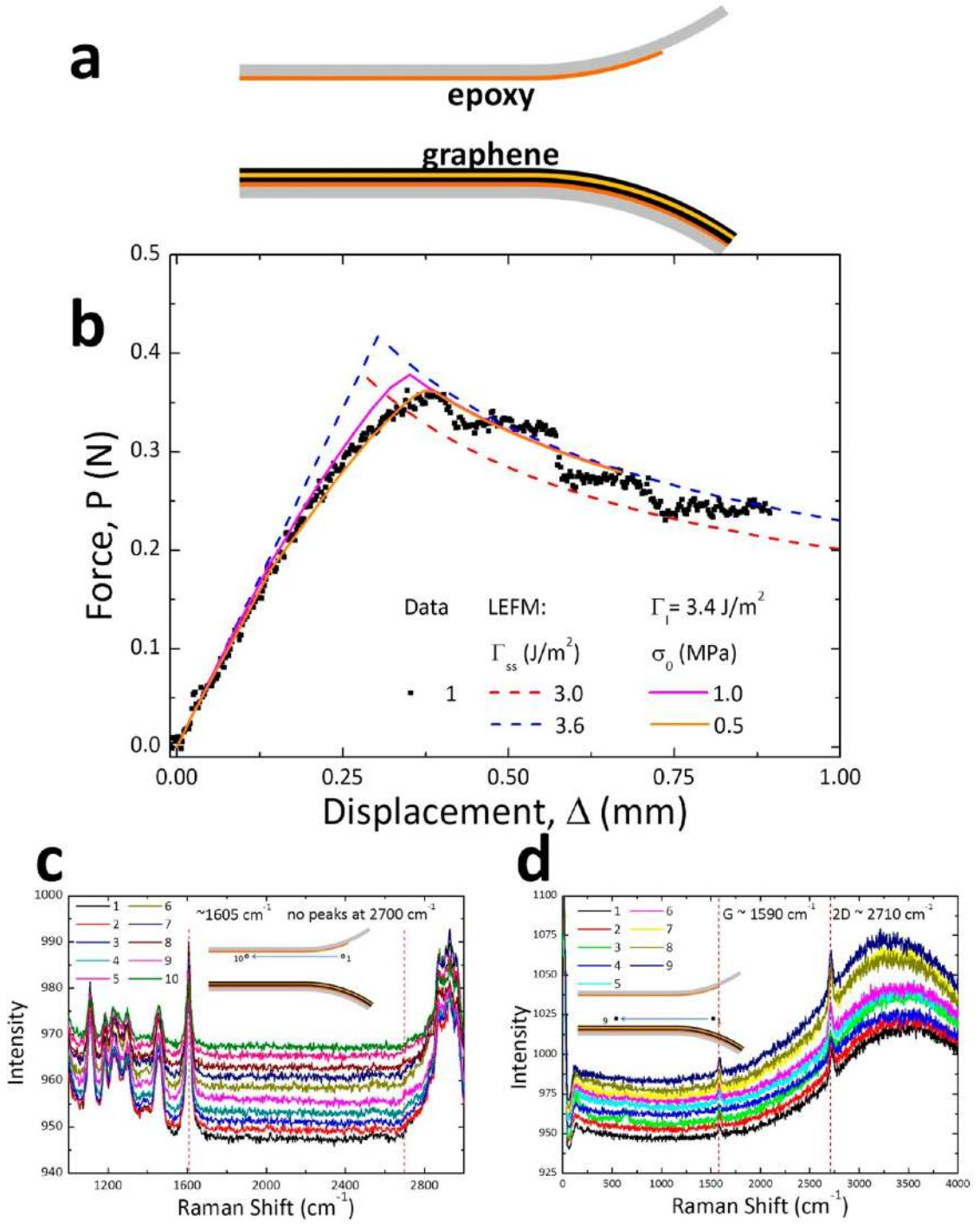

Figure 4. Results of experiments at an applied separation rate of 25.4 μm/s. (a) A schematic of delamination along the graphene/epoxy interface. (b) Force−displacement response of an experiment and associated simulations. (c) Raman spectra of ten spots on the epoxy with no graphene on it. (d) Raman spectra of copper foil after separation; the series of spots from 1 to 9 confirm the presence of graphene because it was not transferred to the epoxy.

Intermediate Cases. The two scenarios presented so far were from applied displacement rates of 254.0 and 25.4 μm/s. As indicated in Table 1, 35 experiments were conducted at the higher rate while 6 were conducted at the lower rate. Experiments were also conducted at intermediate rates of 42.3, 84.6, 127.0, and 169.3 μm/s. These resulted in varying degrees of graphene transfer, with increasingly larger regions of graphene being transferred to the epoxy as the applied displacement rate was increased. This is demonstrated in Figure 5b−d, where SEM images of the fracture surfaces from experiments that were conducted at 42.3, 84.6, and 169.3 μm/s, respectively, are presented. At the lowest rate, three regions from the upper fracture surface are identified: bare silicon, graphene on epoxy and bare epoxy. The boundary between the bare

TABLE 1. A Summary of the Fracture Modes and Occurrence at Each Loading Rate (G = Graphene)

loading rate		25.4 μm/s	42.3 μm/s	84.6 μm/s	127 μm/s	169.3 μm/s	254 μm/s
Main Fracture Path		Epoxy/G	Mixed	Mixed	Mixed	G/Cu foil	G/Cu foil
Total Samples		6	1	1	1	4	35
Continuity of graphene film		0.5 × 4 cm (G on Cu foil)				0.5 × 0.6 cm (G on epoxy)	0.5 × 1.6 cm (G on epoxy)
Frequency of mode	1		1	1		4	23
	2	1			1		
	3—1	4					4
	3—2	1					8

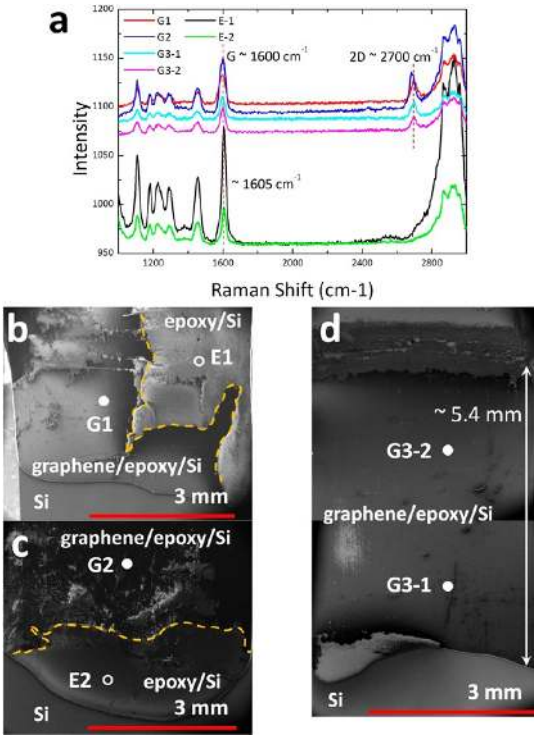

Figure 5. Raman spectra and low-resolution SEM images were prepared to track the transfer of graphene at intermediate loading rates. (a) Raman spectra of the epoxy fracture surface following experiments at 42.3, 84.6, and 169.3 μm/s. (b) Low-resolution SEM image of the epoxy fracture surface following an experiment at 42.3 μm/s which shows small patches of graphene transferred to the epoxy. (c) Low-resolution SEM image of the epoxy fracture surface following experiments at 84.6 μm/s which again shows small patches of graphene. (d) More continuous transfer of graphene (5 × 5.4 mm) was achieved at a loading rate of 169.3 μm/s.

silicon and graphene on epoxy is the epoxy terminus so there was indeed no graphene on the bare silicon. The contrast between the graphene/epoxy and bare epoxy regions above the terminus is clear, with the lack of charging due to the presence of graphene leading to the darker region. This is borne out by the Raman spectra from spots identified as G1 and E1 in Figure 5a. The spectrum from G1 had the G and 2D peaks with an average value of I_{2D}/I_G = 1.1 for graphene, confirming the presence of graphene on epoxy and delamination at the graphene/copper interface. The spectrum from E1 only had the epoxy peak at 1605 cm^{-1}; thus in this region the delamination occurred at the graphene/epoxy interface. At 42.3 μm/s, the patches of graphene on epoxy and bare epoxy were both about 3 × 3 mm^2. The situation at 84.6 μm/s (Figure 4c) was quite similar; the same three regions can be identified in the SEM image, the Raman spectra at the spots G2 and E2 had the same features as those obtained at G1 and E1, and the patches of graphene on epoxy and bare epoxy are about the same size at 3 × 3 mm^2. At 169.3 μm/s, except for a very small patch of bare epoxy, it was a clean transfer of graphene to epoxy over the full width of the silicon strip and up to 5.4 mm from the epoxy terminus. The Raman spectra from the spots confirmed the presence of graphene on epoxy with and average value of I_{2D}/I_G = 1.1.

Two other modes of delamination were observed (Supporting Information Figure S3) in addition to purely graphene/copper (case 1) and graphene/epoxy (case 2) delamination. These involved delamination at both the upper and lower graphene monolayers and are designated cases 3—1 and 3—2 in Supporting Information Figure S3. In the former case, the graphene delaminated from the upper epoxy terminus along the upper graphene/epoxy interface, but this excited an internal delamination at the lower graphene/copper interface, which propagated for a short distance before being overtaken by the delamination at the upper graphene/epoxy interface, at which point the lower delamination arrested. This sequence of events resulted in one and sometimes more copper blisters on the lower silicon strip and, although there was evidence of delamination at the copper/graphene interface, delamination mainly occurred at the graphene/epoxy interface (Supporting Information Figure S3d). In case 3—2, the progression was the same except that the delamination of the lower interface never arrested and outran the delamination at the upper interface. In this case, graphene/epoxy delamination was dominant (Supporting Information Figure S3e) with smaller regions of graphene/copper delamination.

Adhesive Interactions. The measured load—displacement responses associated with delamination along the graphene/copper (Figure 3b) and graphene/epoxy (Figure 4b) interfaces were used to determine the adhesion energy as well as the strength and range of the

interactions associated with each interface. The adhesion energy was first obtained from fracture mechanics concepts[18] using a simple beam analysis to determine the elastic energy available to separate the interfaces of interest. The slope of the rising portion of the load–displacement response was predicted by simple beam theory (see Supporting Information eq S1 in Section 8) and matched the data in the first and subsequent load-unload cycles (Figure 3b) using the measured crack length in each case and the other specimen dimensions and the Young's modulus of the silicon strips. The descending portion of the load–displacement response corresponds to the initiation and growth of the delamination along the graphene/copper interface and is governed in the simplest case by the adhesion energy Γ_{ss} and Supporting Information eq S3. Values of 5 and 7 J/m^2 bounded the measured response in this regime.

These adhesion energy levels are much higher than the value 720 ± 70 mJ/m^2 measured by Yoon *et al.*[11] for the graphene/copper film interface. They are also higher than value 1.8 J/m^2 for an epoxy/silicon interface measured at very low separation rates,[19] but lower than the fracture toughness of graphene itself at 15.9 J/m^2.[20] In separate control experiments (see Supporting Information Section 10) on silicon/epoxy/silicon sandwich specimens, the adhesion energy of the epoxy/silicon interface was 7.5 ± 0.2 and 11.1 ± 0.1 J/m^2 at loading rates of 84.6 and 254.0 μm/s, respectively. These values are higher than the bound of 5–7 J/m^2 at 254.0 μm/s for the graphene/copper foil interface, thereby explaining why delamination at the silicon/epoxy interface never occurred. The result also suggests that, at 254.0 μm/s, the graphene/epoxy interface had higher adhesion energy. The question then arises as to why the adhesion energy is so high. One possibility is that the copper foil and the epoxy were yielding with attendant energy dissipation during delamination growth, thereby adding to the intrinsic adhesion energy of the graphene/copper interface.[21,22]

To address this question, we conducted a series of finite element analyses that accounted for the elastic-plastic behavior of the epoxy and copper foil (Supporting Information Section 9). The conclusion of this exercise was that the intrinsic toughness of the graphene/copper interface was 6.0 J/m^2 and that plastic dissipation in the copper was less than 10%. The strength of the graphene/copper interaction as a function of separation was represented by a traction–separation relation[23] which had a maximum strength of 0.5 MPa and an interaction range of 24.0 μm. This was able to capture the more gradual onset of delamination growth that was observed in the experiments, particularly in cycles 2 and 3 in Figure 3b.

A similar set of analyses were conducted (see Supporting Information Section 8) with a view to modeling the load–displacement response of the experiment conducted at 25.4 μm/s. The traction–separation relation of the graphene/epoxy interface was represented by an intrinsic adhesion energy of 3.4 J/m^2, a maximum strength of 0.5 MPa and interaction range of 13.6 μm (Tables 2 and 3), and again determined that plastic dissipation was minimal.

TABLE 2. Material Properties and Geometry of Each Component

	Young's modulus (GPa)	Poisson's ratio	yield strength (MPa)	thickness (μm)	size (cm × cm)
Silicon	169	0.2	N/A	291 ± 5	0.5 × 4
Epoxy	3.0 ± 0.02	0.4	41.8 ± 2.9		
Graphene	~1000				0.5 × 4
Cu foil	110	0.33	23.3 ± 3.5	31.8 ± 4.8	0.5 × 4

TABLE 3. Values of the Parameters Associated with the Traction–Separation Relations (Supporting Information Figure S8) That Were Extracted by Simulation

interaction pair	TSR	Γ_{ss} (J/m^2)	σ_0 (MPa)	δ_n^0 (μm)	δ_n^c (μm)
Graphene/Cu	1	6	3	0.03	4
	2		0.5	0.005	24
Graphene/epoxy	1	3.4	1	0.01	6.8
	2		0.5	0.005	13.6

Rate Dependence. Thus, at an applied displacement rate of 25.4 μm/s, the strength and adhesion energy of the graphene/epoxy interface fell below those of the graphene/copper interface and delamination along the former interface was favored. This suggests that at least one of the interactions is rate dependent and/or the viscoelastic nature of the epoxy is contributing to the observed overall rate dependence. The rate dependence of the adhesion energy of contact pairs has already been exploited for selective separation in transfer printing.[24,25] Given that the experiments in the present study were conducted at room temperature, well below the glass transition (100 °C) of this epoxy and the local strain rates near the delamination front are higher than the far field value, thereby shifting the epoxy even further into the glassy domain, it is unlikely that bulk viscoelastic effects were at play near the delamination front. It is also unlikely that the interactions between graphene and copper foil are rate dependent, at least in the quasi static regime being considered here. Accordingly, the noted switch in delamination from the graphene/copper foil interface to the graphene/epoxy interface may be attributed to rate dependence of the latter. This could be due to the manner in which the epoxy cures near graphene, leaving a thin region often known as the interphase,[26] whose properties differ from those of the bulk epoxy.

Prior to curing, the viscosity of the epoxy is low, so that it follows the morphology of the graphene grown on the copper foil. This leads to the possibility that surface roughness, in conjunction with an interphase layer, could contribute to the rate dependence of the

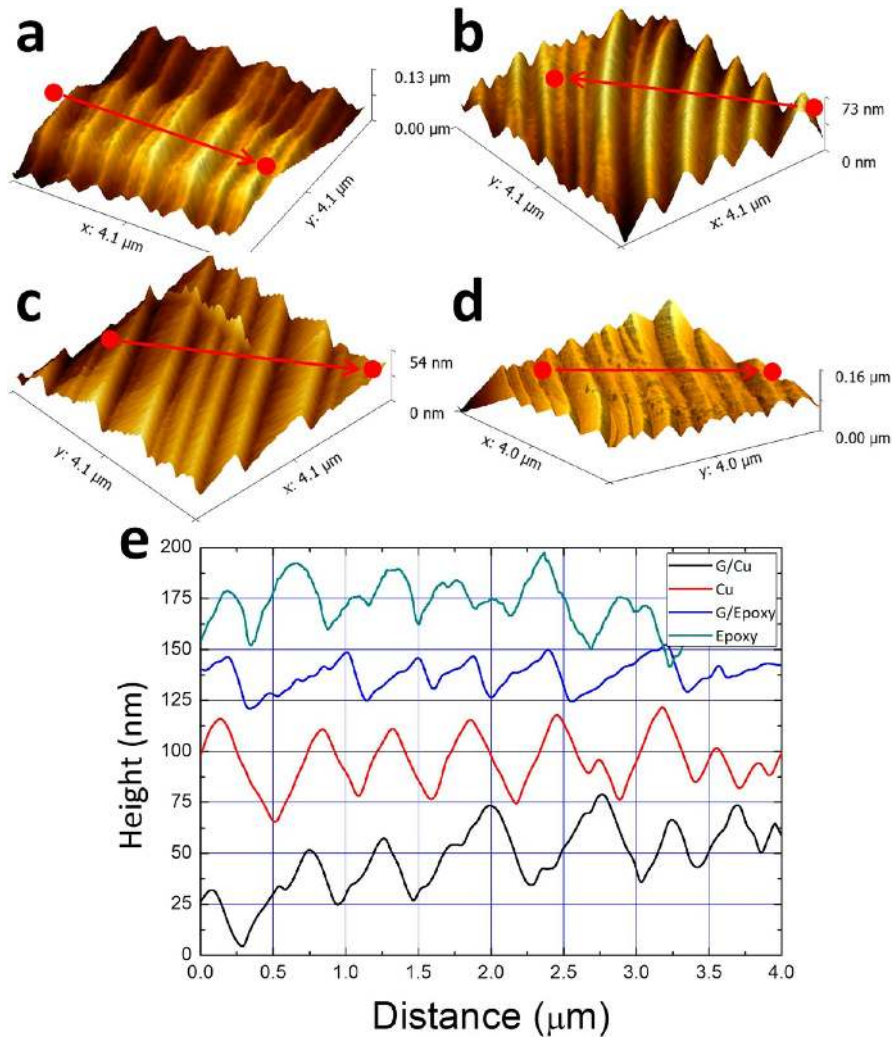

Figure 6. AFM scans prior to and following transfer of graphene. (a) The initial state of graphene on copper foil following deposition. The RMS roughness was 11.4 nm. (b) Copper without graphene after transfer had an RMS roughness of 12.3 nm. (c) The RMS roughness of the graphene-coated epoxy surface was 7.35 nm. (d) The RMS roughness of epoxy without graphene was 11.3 nm. (e) Profiles indicate that the wavelength of the surface roughness was quite similar in all cases.

interaction between graphene and epoxy. The roughness of the graphene on copper foil after deposition (Figure 6a), bare copper foil (Figure 6b) and graphene on epoxy (Figure 6c) after separation along the graphene/copper interface and bare epoxy (Figure 6d) after separation along the graphene/epoxy interface were measured by atomic force microscopy (AFM). These images all display step-like features, which appear to have very similar wavelengths (0.7 μm) and peak to valley heights of about 25 nm (Figure 6e), confirming that both the graphene and epoxy conformed to the surface of the copper foil. These features might be viewed as atomic steps in the copper foil, but the peak to peak variations in surface morphology would be much smaller than the 25 nm observed here, leading to the conclusion that the step-like features were formed at the high temperatures encountered in the CVD process.

Roughness effects may also help reconcile the difference in the 720 $\pm$ 70 mJ/m^2 adhesion energy of the graphene/copper film interface measured by Yoon *et al.*[11] and the 6.0 J/m^2 measured here for the graphene/copper foil interface. The grains of the copper films were about 10 μm in lateral dimension, much smaller than those of the copper foil, and the overall root-mean-squared (RMS) roughness was on the order of 20 nm.[27] Because the copper film was deposited on silicon, this is the only roughness scale. The RMS roughness of the step-like features of the copper foils (Figure 6 and Supporting Information Figure S6e,f) was about 10 nm but there were other features such as scratches (Supporting Information Figure S6c,d) produced during rolling of the foil and undulations associated with rumples in the foil that were produced by folding of the foil around the quartz cylinder and the spring back from subsequent attempts to straighten it out (Supporting Information Figure S1a). The RMS roughness of the scratches was about 140 nm over a 50 $\times$ 70 μm region, while the RMS roughness of the undulations was about 775.9 $\pm$ 186 nm over a square millimeter. The graphene and epoxy were able to

conform to all these varied angular features, meaning that delamination along the graphene/copper foil interface had to follow more complex paths compared to the simpler path for the copper film. Such a range of angularity introduces local variations in fracture mode-mix and greater chances of interlocking of delamination surfaces which could conceivably result in higher adhesion energies.

CONCLUSIONS

It has been demonstrated that it is possible to mechanically separate CVD grown graphene from its copper foil seed layer by bonding the graphene-coated copper foil to silicon strips with an epoxy and then separating the silicon strips in a double cantilever beam configuration at a high enough applied separation rate. For the conditions employed in this study, this had to be equal to or greater than 254.0 μm/s. When the applied displacement rate was an order of magnitude lower, the graphene/epoxy interface delaminated. At intermediate rates, there was a mixture of the two modes. The delamination paths in all the experiments were diagnosed *via* a combination of Raman spectroscopy, scanning electron microscopy and atomic force microscopy.

This result has very important implications for nano manufacturing processes such as roll-to-roll transfer, where loading rates can be controlled so as to produce delamination at the desired interface. Although silicon strips and epoxy were used in this study to effect this selective delamination are not compatible with roll-to-roll devices, other materials that are compatible can be selected using the same fracture mechanics principles that were used to analyze the experiments here.

A fracture mechanics analysis of the load–displacement responses at the two extreme applied displacement rates was used to determine the adhesion energy as well as the strength and range of the interactions between graphene and copper and between graphene and epoxy. At 254.0 μm/s, the adhesion energy of the graphene/copper interface was 6 J/m^2 with a maximum strength and interaction range of 0.5 MPa and 24 μm, respectively. The corresponding values of adhesion energy, maximum strength, and interaction range at 25.4 μm/s were 3.4 J/m^2, 0.5 MPa, and 13.6 μm, respectively, for the graphene/epoxy interface. These values of adhesion energy were surprisingly high and could have been due to significant contributions from plastic energy dissipation in the copper foil and epoxy layers. However, a detailed finite element analysis found very little dissipation in either layer due to the fact that their yield strengths were much higher than the maximum strength of the interfaces. This means that the quoted adhesion energy values actually corresponded to the intrinsic adhesion of the interfaces, although the underlying mechanisms for such high adhesion energy require further study.

The source of the rate dependence remains to be understood and doing so will allow much more definitive analyses of delamination scenarios for roll-to-roll manufacture. Nonetheless, it can be most likely narrowed down to a rate dependence of the graphene/epoxy interface, with an interphase layer of epoxy whose properties are different from those of the bulk epoxy due to the constraint applied by the graphene on the movement of the molecular chains of the epoxy near the graphene as the epoxy was cured.

METHODS

The details of the specimen fabrication are given in sections 1–3 of the Supporting Information. Following CVD growth of graphene on copper foils,[2] the 5 × 5 cm^2 foils were flattened on a silicon wafer (Supporting Information Figure S1a). Each graphene surface was in turn bonded to silicon strips (Supporting Information Figure S1b–d) to form, from bottom to top, a silicon/epoxy/graphene/copper/graphene/epoxy/silicon laminate (Supporting Information Figure S1e). The entire length of the bottom silicon strip was bonded to the lower graphene layer by its epoxy, whereas the upper epoxy layer only bonded about 75% of the upper silicon strip to the upper layer of graphene, thereby producing bimaterial corners or a blunt crack, depending on the scale of observation, at the epoxy terminus (Supporting Information Figure S2). The nominal thickness of each layer is identified in Figure 1a. The final step in preparing the specimen was to bond aluminum tabs (Supporting Information Figure S1f) to each silicon strip. These tabs allowed the laminate to be connected to a servo hydraulic loading device in a classical fracture mechanics test configuration, the double cantilever beam.[18]

The ends of the upper and lower silicon strips were separated (Figure 1a) under displacement control with rates ranging from 25.4 to 254.0 μm/s. The reactive load was measured by a 10 N load cell while the crack tip location was monitored by a camera. With many of the specimens, several load/unload/reload cycles could be conducted before each specimen was completely separated. Both fracture surfaces were then examined with Raman spectroscopy (WITec Alpha 300 micro-Raman confocal microscope, λ = 488 nm) and scanning electron microscopy (SEM; FEI Quanta 650 ESEM) in order to determine the locus of delamination. The latter was particularly useful for mapping the full extent of any transfer of the graphene from its seed copper foil to the adjacent epoxy because the presence of any graphene on the epoxy prevented charging from occurring.

Fracture mechanics analyses of the load–displacement data were used to determine the adhesion energy, strength and range of the interactions between graphene and copper and graphene and epoxy. The details are given in Supporting Information Section 8.

Conflict of Interest: The authors declare no competing financial interest.

Acknowledgment. The authors gratefully acknowledge partial financial support of this work by the National Science Foundation through Grant No. CMMI-1130261. This work is also based upon work supported in part by the National Science Foundation under Cooperative Agreement No. EEC-1160494. R.S.R. furthermore appreciates support from the Institute of Basic Sciences (Republic of Korea). This research was also supported

by Basic Science Research Program through the National Research Foundation of Korea (NRF) funded by the Ministry of Science, ICT & Future Planning (NRF-2014R1A1A1004818). Any opinions, findings and conclusions or recommendations expressed in this material are those of the authors and do not necessarily reflect the views of the National Science Foundation.

Supporting Information Available: The following information is available for interested readers: preparation of silicon strips, preparation of epoxy, fabrication of sandwich specimens, definition of bimaterial corners, identification of delamination modes, high-resolution SEM images of graphene transferred to epoxy, decomposition of Raman peaks, fracture analysis, the tensile stress−strain behavior of epoxy and copper foil, rate dependent adhesion energy of silicon/epoxy interfaces, definition of traction−separation relation parameters, Raman maps for graphene/copper delamination, Raman maps for graphene/epoxy delamination, sheet resistance. This material is available free of charge *via* the Internet at http://pubs.acs.org.

REFERENCES AND NOTES

1. Novoselov, K. S.; Geim, A. K.; Morozov, S. V.; Jiang, D.; Zhang, Y.; Dubonos, S. V.; Grigorieva, I. V.; Firsov, A. A. Electric Field Effect in Atomically Thin Carbon films. *Science* **2004**, *306*, 666–669.
2. Li, X. S.; et al. Large-Area Synthesis of High-Quality and Uniform Graphene Films on Copper Foils. *Science* **2009**, *324*, 1312–1314.
3. Li, X.; Magnuson, C. W.; Venugopal, A.; Tromp, R. M.; Hannon, J. B.; Vogel, E. M.; Colombo, L.; Ruoff, R. S. Large-Area Graphene Single Crystals Grown by Low-Pressure Chemical Vapor Deposition of Methane on Copper. *J. Am. Chem. Soc.* **2011**, *133*, 2816–2819.
4. Li, X.; et al. Graphene Films with Large Domain Size by a Two-Step Chemical Vapor Deposition Process. *Nano Lett.* **2010**, *10*, 4328–4334.
5. Chen, S.; et al. Oxidation Resistance of Graphene-Coated Cu and Cu/Ni Alloy. *ACS Nano* **2011**, *5*, 1321–1327.
6. Commercial Scale Large-Area Graphene Now Available from Bluestone Global Tech in 24″x300″ Films. http://www.azonano.com/news.aspx?newsID=26553.
7. Tao, L.; Lee, J.; Chou, H.; Holt, M.; Ruoff, R. S.; Akinwande, D. Synthesis of High Quality Monolayer Graphene at Reduced Temperature on Hydrogen-Enriched Evaporated Copper (111) Films. *ACS Nano* **2012**, *6*, 2319–2325.
8. Na, S. R.; Suk, J. W.; Ruoff, R. S.; Huang, R.; Liechti, K. M. Ultra Long-Range Interactions between Large Area Graphene and Silicon. *ACS Nano* **2014**, *8*, 11234–11242.
9. Suk, J. W.; Kitt, A.; Magnuson, C. W.; Hao, Y.; Ahmed, S.; An, J.; Swan, A. K.; Goldberg, B. B.; Ruoff, R. S. Transfer of CVD-Grown Monolayer Graphene onto Arbitrary Substrates. *ACS Nano* **2011**, *5*, 6916–6924.
10. Wang, Y.; Zheng, Y.; Xu, X.; Dubuisson, E.; Bao, Q.; Lu, J.; Loh, K. P. Electrochemical Delamination of CVD-Grown Graphene Film: Toward the Recyclable Use of Copper Catalyst. *ACS Nano* **2011**, *5*, 9927–9933.
11. Yoon, T.; Shin, W. C.; Kim, T. Y.; Mun, J. H.; Kim, T.-S.; Cho, B. J. Direct Measurement of Adhesion Energy of Monolayer Graphene As-Grown on Copper and Its Application to Renewable Transfer Process. *Nano Lett.* **2012**, *12*, 1448–1452.
12. Wang, Y. Y.; Ni, Z. H.; Yu, T.; Shen, Z. X.; Wang, H. M.; Wu, Y. H.; Chen, W.; Shen, W.; Thye, A. Raman Studies of Monolayer Graphene: The Substrate Effect. *J. Phys. Chem. C* **2008**, *112*, 10637–10640.
13. He, R.; Zhao, L.; Petrone, N.; Kim, K. S.; Roth, M.; Hone, J.; Kim, P.; Pasupathy, A.; Pinczuk, A. Large Physisorption Strain in Chemical Vapor Deposition of Graphene on Copper Substrates. *Nano Lett.* **2012**, *12*, 2408–2413.
14. Wang, X.; et al. Direct Delamination of Graphene for High-Performance Plastic Electronics. *Small* **2014**, *10*, 694–698.
15. Frank, O.; Vejpravova, J.; Holy, V.; Kavan, L.; Kalbac, M. Interaction between Graphene and Copper Substrate: The role of Lattice Orientation. *Carbon* **2014**, *68*, 440–451.
16. Lee, J. U.; Yoon, D.; Cheong, H. Estimation of Young's Modulus of Graphene by Raman Spectroscopy. *Nano Lett.* **2012**, *12*, 4444–8.
17. Ni, Z. H.; Yu, T.; Lu, Y. H.; Wang, Y. Y.; Feng, Y. P.; Shen, Z. X. Uniaxial Strain on Graphene: Raman Spectroscopy Study and Band-Gap Opening. *ACS Nano* **2008**, *2*, 2301–2305.
18. Kanninen, M. F., Popelar, C. H. *Advanced Fracture Mechanics*; Oxford University Press: Oxford, U.K., 1985.
19. Gowrishankar, S.; Mei, H.; Liechti, K. M.; Huang, R. Comparison of Direct and Iterative Methods for Determination of Silicon/Epoxy Interface Traction-Separation Relations. *Int. J. Fract.* **2012**, *177*, 109–128.
20. Zhang, P. Fracture Toughness of Graphene. *Nat. Commun.* **2014**, *5*, No. 3782.
21. Swadener, J. G.; Liechti, K. M. Asymmetric Shielding Mechanisms in the Mixed-Mode Fracture of a Glass/Epoxy Interface. *J. Appl. Mech.* **1998**, *65*, 25–29.
22. Swadener, J. G.; Liechti, K. M.; de Lozanne, A. L. The Intrinsic Toughness and Adhesion Mechanism of a Glass/Epoxy Interface. *J. Mech. Phys. Solids* **1999**, *47*, 223–258.
23. Needleman, A. An Analysis of Tensile Decohesion along an Interface. *J. Mech. Phys. Solids* **1990**, *38*, 289–324.
24. Lee, K. J.; Motala, M. J.; Meitl, M. A.; Childs, W. R.; Menard, E.; Shim, A. K.; Rogers, J. A.; Nuzzo, R. G. Large Area, Selective Transfer of Microstructured Silicon: A Printing-Based Approach to High-Performance Thin-Film Transistors Supported on Flexible Substrates. *Adv. Mater.* **2005**, *17*, 2332–2336.
25. Feng, X.; Meitl, M. A.; Bowen, A. M.; Huang, Y.; Nuzzo, R. G.; Rogers, J. A. Competing Fracture in Kinetically Controlled Transfer Printing. *Langmuir* **2007**, *23*, 12555–12560.
26. Sharpe, L. H. The Interphase in Adhesion. *J. Adhes.* **1972**, *4*, 51–64.
27. Yoon, T.Adhesion Energy Measurement and Interfacial Reliablity Evaluation. MS Thesis, KAIST, Korea, 2013.